A new model for rough surface scattering

Tanos M. Elfouhaily and Joel T. Johnson, *Senior Member, IEEE*

***Abstract*— A new model for rough surface scattering is presented; the model has a form similar to the Small Slope Approximation (SSA) of Voronovich, but with modified kernel functions. As with the SSA, when including two field series terms in the solution the model matches the first and second order small perturbation method in the low frequency limit. Unlike the SSA, the model also achieves agreement with the Kirchhoff Approximation in the high frequency limit even for penetrable surfaces. It is also shown that the new model achieves first order tilt invariance for first order SPM predictions. The new model is derived based on a previous extension of the local curvature approximation (LCA) to third order; the new model is termed the "reduced local curvature approximation of third order" (RLCA3) for this reason. Sample results for scattering from dielectric surfaces are presented to illustrate the new model and its relationship with other theories of rough surface scattering.**

***Index Terms*— Rough Surface Scattering**

I. Introduction

RECENT years have seen the development of an impressive number of theories of rough surface scattering; many of these theories attempt to bridge between the classical Kirchhoff Approach (KA, the high frequency limit) and the small perturbation method (SPM, the low frequency limit). Reference [1] provides a detailed review of many of these models.

The small slope approximation (SSA) of Voronovich [2]-[4] has been shown to be an effective model for surface scattering in several studies. The SSA theory expresses scattered fields as a series in surface "quasi-slope"; a true slope dependence is obtained only in the high frequency limit. The first field series term has a form similar to the field predictions of the Kirchhoff approximation (KA), although the Kirchhoff integration is multiplied by a modified function of the incidence and scattering angles. The second field series term includes an additional Fourier integration over the surface Fourier transform multiplied by an SSA kernel function. While this additional integration complicates computation of the two-term SSA field solution, the computational costs are manageable in many cases, and several studies (for example, [5]) have reported results using both terms. Evaluations of the third or higher order SSA field series terms have yet to be reported.

The SSA model is attractive because it is derived to automatically satisfy several fundamental properties, including horizontal and vertical shift invariance, reciprocity, and compliance with the SPM up to second order when both field series terms are included. It has also been shown that the SSA achieves "tilt invariance" in the first order SPM limit to first order in surface tilt angle [6]; this is attractive for remote sensing applications because it implies that the SSA theory should approximate the "two-scale" or composite surface model in sea scattering studies.

While references [2]-[4] also report that the SSA model with two field series terms achieves agreement with the Kirchhoff approximation in the high frequency limit, the surface boundary conditions considered in the references included only the Dirichlet, Neumann, and perfectly conducting cases (i.e. impenetrable boundaries). Recent studies [5], [7] have shown that the SSA model fails to achieve agreement with the KA when penetrable surfaces are considered, with significant errors observed particularly in vertical polarization.

An alternative form of the SSA called the "local curvature approximation" (LCA) has also been developed in recent years [8]. The LCA is functionally identical to the SSA, but uses the KA as the first field series term combined with a modified kernel function in the second field series term. Reference [8] presented both these field series terms, and demonstrated that the two term theory (LCA2) could achieve agreement with the SPM1 (including tilt invariance to first order in surface tilt) as well as the KA. However, the model did not achieve agreement with the SPM2. It has been shown that this is a particular limitation in evaluating cross-polarized backscattering, due to the strong influence of the second order SPM kernel for this polarization [9].

In reference [9], the original LCA model was modified to improve its tilt invariance properties, and to extend the theory to include a third field series term. The resulting LCA3 model achieved compliance with KA, SPM1, and SPM2, with the latter two limits reached regardless of the tilt angle to a tilted frame of reference. Inclusion of the third field series term is required in order to achieve any of the SPM2 limit; because this third field series term requires yet another Fourier integration beyond that of the second field series term, computational complexity limits use of this method in most practical applications. When only two field series terms are included, the SPM2 limit is not reached, but SPM1 is reached to arbitrary order in slope for a tilted frame of reference. In order to achieve the SPM2 limit when including only two field series terms, the requirement that the model reach SPM1 to arbitrary order in surface tilt must be relaxed.

In this paper, a "reduced" version of the LCA3 theory is presented that achieves the KA, SPM1, and SPM2 limits while requiring use of only two field series terms. The theory retains tilt invariance to first order in surface tilt for the SPM1 limit. Due to these properties, the theory should have reasonably wide applicability to rough surface scattering problems of interest in remote sensing. The new model is called the "reduced local curvature approximation of third order" (RLCA3). The next section provides a description of the notation to be utilized, while Section III describes the RLCA3

Manuscript received Month dd, yyyy; revised Month dd, yyyy. T. M. Elfouhaily is with the Rosenstiel School of Marine and Atmospheric Science, University of Miami. J. T. Johnson is with The Ohio State University, Dept. of Electrical and Computer Engineering and ElectroScience Laboratory.

equations. Properties of the RLCA3 equations are verified in Section IV, and practical issues involved in computing RLCA3 predictions are discussed in Section V. Section VI provides example results involving scattering from penetrable, Gaussian correlation function surfaces, and compares RLCA3 predictions with those from the SSA and LCA2 theories. Other extensions of the RLCA3 and SSA theories are discussed in Section VII, and final conclusions are presented in Section VIII.

II. Basic Formulation and Notation

The notation utilized in this paper is similar to that introduced in [9], and is briefly reviewed in this Section. Because the LCA3 kernels to be used involve a tilting process, the notation utilized is somewhat distinct from that of other rough surface scattering studies.

The problem considered involves a time harmonic electromagnetic wave propagating in vacuum that encounters an interface (Σ) with a half-space of relative permittivity ϵ. The scattering problem is described by the propagation directions of the incident and scattered waves in the free space region, here labeled $\boldsymbol{K}_0$ and $\boldsymbol{K}$, respectively. These are three dimensional vectors; reference to "horizontal" and "vertical" parts of these vectors implies choice of a coordinate system. In order to simplify the discussion of tilt invariance, notations are adopted in this paper that attempt to make any coordinate system dependencies explicit. The vector $\boldsymbol{Q}$ is defined as $\boldsymbol{K} - \boldsymbol{K}_0$, and the wavenumber in the vacuum medium is denoted by K.

The scattered field above and far away from the surface is related to the incident one through the scattering operator which reads in dyadic notation (in the far field at $R \to \infty$),

$$\boldsymbol{E}_s(\boldsymbol{R}) = \frac{\mathrm{i}\mathrm{e}^{\mathrm{i}KR}}{2\pi R}\mathbf{S}(\boldsymbol{K}, \boldsymbol{K}_0) \cdot \boldsymbol{E}_0, \tag{1}$$

which is a direct consequence of the Weyl representation of the Green's function. Here the incident plane wave field is written as

$$\boldsymbol{E}_i \;=\; \boldsymbol{E}_0 e^{i\boldsymbol{K}_0 \cdot \boldsymbol{R}} \tag{2}$$

on the surface boundary. The dyad $\mathbf{S}(\boldsymbol{K}, \boldsymbol{K}_0)$ is termed the scattering amplitude in what follows. This scattering amplitude when computed exactly is independent of the coordinate system used to describe the scattering problem.

For electromagnetic scattering problems, it is convenient to define horizontal ($\hat{\boldsymbol{H}}$) and vertical ($\hat{\boldsymbol{V}}$) polarization unit vectors. To avoid reference to a particular coordinate system, polarization vectors are defined as

$$\hat{\boldsymbol{H}}_{\boldsymbol{i}} \;=\; \hat{\boldsymbol{K}} \times \hat{\boldsymbol{K}}_{\mathbf{0}} / \left| \hat{\boldsymbol{K}} \times \hat{\boldsymbol{K}}_{\mathbf{0}} \right| \tag{3}$$

$$\hat{\boldsymbol{H}}_{\boldsymbol{s}} \;=\; \hat{\boldsymbol{H}}_{\boldsymbol{i}} \tag{4}$$

$$\hat{\boldsymbol{V}}_{\boldsymbol{i}} \;=\; \hat{\boldsymbol{H}}_{\boldsymbol{i}} \times \hat{\boldsymbol{K}}_{\mathbf{0}} \tag{5}$$

$$\hat{\boldsymbol{V}}_{\boldsymbol{s}} \;=\; \hat{\boldsymbol{H}}_{\boldsymbol{s}} \times \hat{\boldsymbol{K}} \tag{6}$$

where the subscripts i and s refer to the incident and scattered field, respectively. Problems involving backscattering require independent specification of the polarization vectors, which can be chosen perpendicular to the incident direction in any manner deemed preferable.

These definitions allow the dyadic properties of $\mathbf{S}(\boldsymbol{K}, \boldsymbol{K}_0)$ to be written as

$$\begin{aligned}\mathbf{S}(\boldsymbol{K}, \boldsymbol{K}_0) \;=\;& \hat{\boldsymbol{H}}_{\boldsymbol{s}} S_{HH} \hat{\boldsymbol{H}}_{\boldsymbol{i}} + \hat{\boldsymbol{V}}_{\boldsymbol{s}} S_{VH} \hat{\boldsymbol{H}}_{\boldsymbol{i}} + \\ & \hat{\boldsymbol{H}}_{\boldsymbol{s}} S_{HV} \hat{\boldsymbol{V}}_{\boldsymbol{i}} + \hat{\boldsymbol{V}}_{\boldsymbol{s}} S_{VV} \hat{\boldsymbol{V}}_{\boldsymbol{i}}\end{aligned} \tag{7}$$

where the left unit vectors represent the scattered field polarization and the right unit vectors are dotted into the polarization of the incident field in equation (1). This polarization basis is utilized for all dyadic quantities in what follows.

In some cases (for example, in the SPM) specification of a coordinate system is unavoidable when describing the scattering amplitude. In this case, the coordinate system utilized is described by a normal vector $\hat{\boldsymbol{n}}$, which represents the "vertical" direction in the chosen coordinate system (i.e. $\hat{\boldsymbol{n}}$ points from the surface into the vacuum region.) In this case, "perpendicular" and "parallel" projection operators can be defined as

$$\mathbf{P}_{\perp}(\hat{\boldsymbol{n}}) \;=\; \hat{\boldsymbol{n}}\hat{\boldsymbol{n}} \tag{8}$$

$$\mathbf{P}_{\parallel}(\hat{\boldsymbol{n}}) \;=\; \mathbf{I} - \hat{\boldsymbol{n}}\hat{\boldsymbol{n}} \tag{9}$$

where $\mathbf{I}$ is the identity dyad. These dyads produce the vector perpendicular and parallel components, respectively, when multiplying a specified vector. When choice of a coordinate system is implied in the definition of a scattering amplitude, the scattering amplitude is written as $\mathbf{S}(\boldsymbol{K}, \boldsymbol{K}_0|\hat{\boldsymbol{n}})$.

For simplicity in what follows, we will often choose $\hat{\boldsymbol{n}} = \hat{z}$, assuming that the $\hat{z}$ direction is defined to be the "vertical" direction in the coordinate system of interest. In this case, the x and y coordinates in a Cartesian system represent the horizontal coordinates. In such cases a three dimensional position vector on the surface $\boldsymbol{R}$ can be written as $\boldsymbol{r} + \hat{z}h(\boldsymbol{r})$, where $h(\boldsymbol{r})$ is the function the represents the surface height. We can also define the Fourier transform of this surface through

$$h(\xi_x, \xi_y) \;=\; \left(\frac{1}{2\pi}\right)^2 \int \mathrm{e}^{-\mathrm{i}(\xi_x x + \xi_y y)}\; h(x, y)\; \mathrm{d}x\mathrm{d}y$$

with the inverse transform given by

$$h(x, y) \;=\; \int \mathrm{e}^{\mathrm{i}(\xi_x x + \xi_y y)}\; h(\xi_x, \xi_y)\; \mathrm{d}\xi_x \mathrm{d}\xi_y \tag{10}$$

III. The Reduced Local Curvature Approximation of third order

The RLCA3 has a functional structure identical to that of the SSA, and is expressed up to second "curvature order" as

$$\mathbf{S}(\boldsymbol{K}, \boldsymbol{K}_0|\hat{z}) \;\approx\; \mathbf{S}_0(\boldsymbol{K}, \boldsymbol{K}_0|\hat{z}) + \mathbf{S}_1(\boldsymbol{K}, \boldsymbol{K}_0|\hat{z}) \tag{11}$$

where

$$\mathbf{S}_0(\boldsymbol{K}, \boldsymbol{K}_0|\hat{z}) \;=\; \frac{\boldsymbol{\mathcal{K}}(\boldsymbol{K}, \boldsymbol{K}_0)}{Q_z} \int \mathrm{d}x\; \mathrm{d}y\; \mathrm{e}^{-\mathrm{i}\boldsymbol{Q}\cdot\boldsymbol{R}} \tag{12}$$

$$\begin{aligned}\mathbf{S}_1(\boldsymbol{K}, \boldsymbol{K}_0|\hat{z}) \;=\;& -\mathrm{i} \int \mathrm{d}x\; \mathrm{d}y\; \mathrm{e}^{-\mathrm{i}\boldsymbol{Q}\cdot\boldsymbol{R}} \\ & \int \mathrm{d}\xi_x\; \mathrm{d}\xi_y\; \mathrm{e}^{\mathrm{i}(\xi_x x + \xi_y y)} h(\xi_x, \xi_y) \\ & \mathbf{T}_1^{'}(\boldsymbol{K}, \boldsymbol{K}_0; \boldsymbol{\xi}, \boldsymbol{Q}_{\boldsymbol{H}} - \boldsymbol{\xi})\end{aligned} \tag{13}$$

with

$$\boldsymbol{\xi} = \hat{x}\xi_x + \hat{y}\xi_y \tag{14}$$

and

$$\boldsymbol{Q_H} - \boldsymbol{\xi} = \hat{x}(Q_x - \xi_x) + \hat{y}(Q_y - \xi_y) \tag{15}$$

The $|\hat{z}$ notation in the scattering amplitudes above indicates that the equations are written in a coordinate system in which $\hat{z}$ is regarded as normal to the mean surface plane, so that x and y are the horizontal coordinates as discussed previously. The functional form of the RLCA3 is also identical to that of the two term LCA series in [9], except that the kernel $\mathbf{T}_1^{'}$ of the RLCA3 becomes the $\mathbf{T}_1$ kernel of [9] in the LCA model of [9]. The first term is the Kirchhoff Approximation, with $\mathbf{K}$ representing the Kirchhoff kernel function; detailed equations for this kernel are provided in the appendix.

The new RLCA3 kernel is specified through

$$\begin{aligned}\mathbf{T}_1^{'}(\boldsymbol{K}, \boldsymbol{K}_0; \boldsymbol{\xi}^{(1)}, \boldsymbol{\xi}^{(2)}) &= \mathbf{T}_1(\boldsymbol{K}, \boldsymbol{K}_0; \boldsymbol{\xi}^{(1)}) + \\ &\quad \frac{1}{2}\mathbf{T}_2(\boldsymbol{K}, \boldsymbol{K}_0; \boldsymbol{\xi}^{(1)}, \boldsymbol{\xi}^{(2)})\end{aligned} \tag{16}$$

with $\mathbf{T}_1$ and $\mathbf{T}_2$ as specified in [9]; note both are functions of general three dimensional vector arguments. Specific values for these arguments are set by the integrations of equation (13).

In particular, these kernels are given by [9]:

$$\begin{aligned}\mathbf{T}_1(\boldsymbol{K}, \boldsymbol{K}_0; \boldsymbol{\xi}) &= \mathbf{B}\left(\boldsymbol{K}, \boldsymbol{K}_0 | \hat{\boldsymbol{n}} = \frac{\boldsymbol{Q} - \boldsymbol{\xi}}{|\boldsymbol{Q} - \boldsymbol{\xi}|}\right) - \\ &\quad \boldsymbol{\mathcal{K}}(\boldsymbol{K}, \boldsymbol{K}_0)\end{aligned} \tag{17}$$

and

$$\begin{aligned}&\mathbf{T}_2(\boldsymbol{K}, \boldsymbol{K}_0; \boldsymbol{\xi}^{(1)}, \boldsymbol{\xi}^{(2)}) = \left[\frac{\hat{\boldsymbol{n}}^{'} \cdot \boldsymbol{Q}}{\hat{\boldsymbol{n}}^{'} \cdot \left(\boldsymbol{Q} - \boldsymbol{\xi}^{(1)} - \boldsymbol{\xi}^{(2)}\right)}\right] \Bigg\{ \\ &\mathbf{B}_2\left(\boldsymbol{K}, \boldsymbol{K}_0; \boldsymbol{K} - \boldsymbol{\xi}^{(1)} | \hat{\boldsymbol{n}} = \hat{\boldsymbol{n}}^{'}\right) + \\ &\mathbf{B}_2\left(\boldsymbol{K}, \boldsymbol{K}_0; \boldsymbol{K} - \boldsymbol{\xi}^{(2)} | \hat{\boldsymbol{n}} = \hat{\boldsymbol{n}}^{'}\right) - \\ &\mathbf{B}\left(\boldsymbol{K}, \boldsymbol{K}_0 | \hat{\boldsymbol{n}} = \hat{\boldsymbol{n}}^{'}\right)\Bigg\} + \\ &\mathbf{T}_1(\boldsymbol{K}, \boldsymbol{K}_0; \boldsymbol{\xi}^{(1)} + \boldsymbol{\xi}^{(2)}) - \\ &\mathbf{T}_1(\boldsymbol{K}, \boldsymbol{K}_0; \boldsymbol{\xi}^{(1)}) - \mathbf{T}_1(\boldsymbol{K}, \boldsymbol{K}_0; \boldsymbol{\xi}^{(2)})\end{aligned} \tag{18}$$

where

$$\hat{\boldsymbol{n}}^{'} = \frac{\boldsymbol{Q} - \boldsymbol{\xi}^{(1)} - \boldsymbol{\xi}^{(2)}}{\left|\boldsymbol{Q} - \boldsymbol{\xi}^{(1)} - \boldsymbol{\xi}^{(2)}\right|} \tag{19}$$

In the above equations, $\mathbf{B}(\boldsymbol{K}, \boldsymbol{K}_0 | \hat{\boldsymbol{n}})$ and $\mathbf{B}_2(\boldsymbol{K}, \boldsymbol{K}_0; \boldsymbol{\xi} | \hat{\boldsymbol{n}})$ refer to the first and second order kernels of the small perturbation method, respectively, evaluated in a coordinate system where the specified value of $\hat{\boldsymbol{n}}$ is regarded as the vertical direction. Specific equations for $\mathbf{B}$ and $\mathbf{B}_2$ are also provided in the appendix. Equations (16)-(19) show that the RLCA3 model involves SPM kernel functions evaluated in a frame of reference tilted from the original $\hat{z}$ vertical direction of the scattering amplitude. However, the specific choices for $\boldsymbol{\xi}^{(1)}$ and $\boldsymbol{\xi}^{(2)}$ used in equation (13) result in SPM2 kernel functions being evaluated only in the original $\hat{z}$ frame of reference.

IV. Properties of the RLCA3 theory

The RLCA3 formulation inherits the majority of its properties from the two-term LCA3 theory in [9]. Useful properties of the LCA3 kernels in this process are

$$\mathbf{T}_1(\boldsymbol{K}, \boldsymbol{K}_0; \boldsymbol{0}) = 0 \tag{20}$$

$$\nabla \mathbf{T}_1(\boldsymbol{K}, \boldsymbol{K}_0; \boldsymbol{0}) = 0 \tag{21}$$

$$\mathbf{T}_2(\boldsymbol{K}, \boldsymbol{K}_0; \boldsymbol{\xi}^{(1)}, \boldsymbol{0}) = 0 \tag{22}$$

$$\boldsymbol{\nabla}_1 \boldsymbol{\nabla}_2 \mathbf{T}_2(\boldsymbol{K}, \boldsymbol{K}_0; \boldsymbol{0}, \boldsymbol{0}) = 0 \tag{23}$$

$$\mathbf{T}_2(\boldsymbol{K}, \boldsymbol{K}_0; \boldsymbol{\xi}^{(1)}, \boldsymbol{0}) = \mathbf{T}_2(\boldsymbol{k}, \boldsymbol{k}_0; \boldsymbol{0}, \boldsymbol{\xi}^{(2)}) = 0 \tag{24}$$

$$\mathbf{T}_2(\boldsymbol{K}, \boldsymbol{K}_0; \boldsymbol{\xi}^{(1)}, \boldsymbol{\xi}^{(2)}) = \mathbf{T}_2(\boldsymbol{K}, \boldsymbol{K}_0; \boldsymbol{\xi}^{(2)}, \boldsymbol{\xi}^{(1)}) \tag{25}$$

The latter four equations ensure that all constant, linear, and quadratic terms in a Taylor series expansion of $\mathbf{T}_2$ about the origin vanish.

In fact the RLCA3 equations are identical to the two-term LCA3 theory, except for the inclusion of the $\mathbf{T}_2$ term in the modified kernel $\mathbf{T}_1^{'}$. It is straight forward to show following [9] that the RLCA3 remains reciprocal, and that it remains shift invariant because

$$\mathbf{T}_1^{'}(\boldsymbol{K}, \boldsymbol{K}_0; \hat{x}\xi_x + \hat{y}\xi_y, \hat{x}(Q_x - \xi_x) + \hat{y}(Q_y - \xi_y)) \tag{26}$$

still vanishes for $(\xi_x, \xi_y) = (0, 0)$. In order to meet the first order SPM limit in an untilted coordinate system, we need

$$\begin{aligned}\mathbf{T}_1^{'}(\boldsymbol{K}, \boldsymbol{K}_0; \hat{x}Q_x + \hat{y}Q_y, \boldsymbol{0}) &= \mathbf{T}_1(\boldsymbol{K}, \boldsymbol{K}_0; \hat{x}Q_x + \hat{y}Q_y) \\ &= \mathbf{B}(\boldsymbol{K}, \boldsymbol{K}_0 | \hat{z}) - \boldsymbol{\mathcal{K}}(\boldsymbol{K}, \boldsymbol{K}_0)\end{aligned} \tag{27}$$

This is easily shown to be true since $\mathbf{T}_2$ vanishes when either argument is zero, and since

$$\hat{z} = \frac{\boldsymbol{Q} - \boldsymbol{\xi}^{'}}{\left|\boldsymbol{Q} - \boldsymbol{\xi}^{'}\right|} \tag{28}$$

when

$$\boldsymbol{\xi}^{'} = \hat{x}Q_x + \hat{y}Q_y \tag{29}$$

To meet the second order SPM limit in an untilted coordinate system, we need

$$\begin{aligned}&\mathbf{T}_1^{'}(\boldsymbol{K}, \boldsymbol{K}_0; \boldsymbol{\xi}^{'}, \boldsymbol{\xi}^{''}) + \mathbf{T}_1^{'}(\boldsymbol{K}, \boldsymbol{K}_0; \boldsymbol{\xi}^{''}, \boldsymbol{\xi}^{'}) = \\ &\mathbf{B}_2\left(\boldsymbol{K}, \boldsymbol{K}_0; \boldsymbol{K} - \boldsymbol{\xi}^{'} | \hat{z}\right) + \mathbf{B}_2\left(\boldsymbol{K}, \boldsymbol{K}_0; \boldsymbol{K}_0 + \boldsymbol{\xi}^{'} | \hat{z}\right) - \\ &\boldsymbol{\mathcal{K}}(\boldsymbol{K}, \boldsymbol{K}_0)\end{aligned} \tag{30}$$

where

$$\boldsymbol{\xi}^{'} = \hat{x}\xi_x + \hat{y}\xi_y \tag{31}$$

$$\boldsymbol{\xi}^{''} = \hat{x}(Q_x - \xi_x) + \hat{y}(Q_y - \xi_y)) \tag{32}$$

This is also satisfied, since $\hat{\boldsymbol{n}}'$ used in evaluating the $\mathbf{T}_2$ kernel also becomes $\hat{z}$ in this case, and since the $\mathbf{T}_1$ terms included in the definition of $\mathbf{T}_2$ cancel the contributions of the $\mathbf{T}_1$ term in equation (16).

Since the original two-term LCA2 theory already achieves compliance with the Kirchhoff Approximation in the high frequency limit, we need to ensure that the contributions of the $\mathbf{T}_2$ term in equation (16) do not distort the original series properties. High frequency contributions in equation (13) are determined through an expansion of the $\mathbf{T}_1'$ kernel in a power series in $\boldsymbol{\xi}$ about the origin of the $\boldsymbol{\xi}$ plane; this is sensible since in the high frequency limit, only surface spectral content for small values of $\boldsymbol{\xi}$ (i.e. large scale surface features) are expected to contribute. Because the $\mathbf{T}_2$ term included in $\mathbf{T}_1'$ vanishes when any of its arguments are zero, and also because the gradient of the $\mathbf{T}_2$ term also vanishes when either argument is 0, the RLCA3 theory retains compliance with the KA theory in the high frequency limit; any corrections to the KA theory are on the order of the surface curvature, rather than slope [9].

Finally, it is of interest to examine the tilt invariance properties of the RLCA3 model. The two term LCA3 theory achieves tilt invariance for the SPM1 to arbitrary order in surface tilt angle. It can be shown following the procedure of [9] that the RLCA3 model distorts these properties so that the SPM1 limit is achieved only to first order in surface tilt angle. No tilt invariance of the SPM2 is obtained, since the SPM2 kernels in the RLCA3 model are always evaluated in the original coordinate system. The RLCA3 model essentially has traded the arbitrary order in slope tilt properties of the LCA2 of [9] for the SPM2 limit in the non-tilted case. The SSA also achieves tilt invariance of the SPM1 only to first order in the surface tilt angle [6].

V. Computation of RLCA3 Cross Sections

Because the RLCA3 retains a form identical to the SSA, normalized radar cross section (NRCS) computations are also identical once the appropriate kernel functions are modified. Under the assumption of a Gaussian random process surface (specified entirely by its covariance function), it is possible to obtain an expression for the expected value of the NRCS. A detailed derivation is provided in [10] and the final expressions for the SSA are available in [5]. Because the RLCA3 has a two term series for scattered fields, normalized radar cross sections involve the power in each of these terms and the correlation between the two. Thus, three cross section terms are obtained, these are labeled $\sigma^{00}_{\alpha\beta}$, $\sigma^{01}_{\alpha\beta}$, and $\sigma^{11}_{\alpha\beta}$ in what follows for contributions of the first field series term squared, the correlation term, and the second field series term squared, respectively. Here α and β represent the scattered and incident polarizations, respectively, and are chosen from H for horizontal or V for vertical. The final expressions are:

$$\sigma^{00}_{\alpha\beta} = \frac{1}{\pi}\left|\frac{\boldsymbol{\mathcal{K}}(\boldsymbol{K},\boldsymbol{K}_0)}{Q_z}\right|^2 \mathcal{H}\{1\} \tag{33}$$

$$\sigma^{01}_{\alpha\beta} = -\frac{2}{\pi}\mathrm{Re}\Big\{\boldsymbol{\mathcal{K}}(\boldsymbol{K},\boldsymbol{K}_0) \Big[\mathcal{H}\{U_{\alpha\beta}(x,y)\} + \mathrm{e}^{-Q_z^2h_0^2}\mathcal{F}\{U_{\alpha\beta}(x,y)\} - U_{\alpha\beta}(0,0)\mathcal{H}\{1\}\Big]\Big\} \tag{34}$$

$$\sigma^{11}_{\alpha\beta} = \frac{1}{\pi}\Big\{\mathcal{H}\{V_{\alpha\beta}(x,y)\} + \mathrm{e}^{-Q_z^2h_0^2}\mathcal{F}\{V_{\alpha\beta}(x,y)\} + Q_z^2\left|U_{\alpha\beta}(0,0)\right|^2\mathcal{H}\{1\}\Big\} \tag{35}$$

The operators $\mathcal{F}$ and $\mathcal{H}$ above are defined as

$$\mathcal{F}\{f(x,y)\} = \int_{-\infty}^{\infty}dx\int_{-\infty}^{\infty}dy\ \mathrm{e}^{\mathrm{i}Q_xx}\mathrm{e}^{\mathrm{i}Q_yy}\ f(x,y) \tag{36}$$

$$\mathcal{H}\{f(x,y)\} = \int_{-\infty}^{\infty}dx\int_{-\infty}^{\infty}dy\ \mathrm{e}^{\mathrm{i}Q_xx}\mathrm{e}^{\mathrm{i}Q_yy}\ D(x,y)\ f(x,y) \tag{37}$$

where the term $D(x,y)$ is given by

$$D(x,y) = \mathrm{e}^{-Q_z^2h_0^2(1-C(x,y))} - \mathrm{e}^{-Q_zh_0^2} \tag{38}$$

Here $C(x,y)$ represents the correlation function of the Gaussian random process surface, and h_0 is the rms height of the rough surface. The term $V_{\alpha\beta}(x,y)$ is given by

$$\begin{aligned} V_{\alpha\beta}(x,y) &= U^{(1)}_{\alpha\beta}(x,y) + Q_z^2U_{\alpha\beta}(x,y)U^*_{\alpha\beta}(-x,-y) \\ &- Q_z^2U_{\alpha\beta}(0,0)U^*_{\alpha\beta}(-x,-y) \\ &- Q_z^2U^*_{\alpha\beta}(0,0)U_{\alpha\beta}(x,y) \end{aligned} \tag{39}$$

Finally, the $U_{\alpha\beta}(x,y)$ and $U^{(1)}_{\alpha\beta}(x,y)$ functions above are given by two-dimensional Fourier transforms of the surface power spectrum, $W(\xi_x,\xi_y)$, and the RLCA3 kernel function:

$$U_{\alpha\beta}(x,y) = \int_{-\infty}^{\infty}d\xi_x\int_{-\infty}^{\infty}d\xi_y\ e^{\mathrm{i}\xi_xx}e^{\mathrm{i}\xi_yy} \mathbf{T}'^{*}_{1,\alpha\beta}(\boldsymbol{K},\boldsymbol{K}_0;\boldsymbol{\xi},\boldsymbol{Q_H}-\boldsymbol{\xi})W(\xi_x,\xi_y) \tag{40}$$

$$U^{(1)}_{\alpha\beta}(x,y) = \int_{-\infty}^{\infty}d\xi_x\int_{-\infty}^{\infty}d\xi_y\ e^{\mathrm{i}\xi_xx}e^{\mathrm{i}\xi_yy} \left|\mathbf{T}'^{*}_{1,\alpha\beta}(\boldsymbol{K},\boldsymbol{K}_0;\boldsymbol{\xi},\boldsymbol{Q_H}-\boldsymbol{\xi})\right|^2 W(\xi_x,\xi_y) \tag{41}$$

where * denotes complex conjugation, and $\boldsymbol{\xi}$ and $\boldsymbol{Q_H}-\boldsymbol{\xi}$ are as specified in equations (14)-(15). The surface power spectrum is normalized so that

$$W(Q_x,Q_y) = \frac{1}{(2\pi)^2}\mathcal{F}\left\{h_0^2C(x,y)\right\} \tag{42}$$

The first NRCS term is identical to the NRCS prediction of the Kirchhoff approximation; the spatial integration involved can be further simplified for particular surface correlation functions, or can be performed numerically for general surfaces. The second NRCS term requires evaluation of $U_{\alpha\beta}$

from equation (40) before the spatial integration can be performed, and therefore apparently involves a four-dimensional integration. However, if the $U_{\alpha\beta}$ function is first evaluated using a Fast Fourier Transform (FFT) before proceeding to the spatial integration, the spatial and spectral integrations become decoupled, and only two two-dimensional integrations are necessary. Similar comments apply for evaluation of the third cross section term, although in this case, FFT computations are necessary for both $U_{\alpha\beta}$ and $U^{(1)}_{\alpha\beta}$ before the spatial integration can be performed. Overall, if a total of N points are used in the spatial integration, the computation of all three NRCS terms can be completed in the order of N operations.

When evaluating RLCA3 NRCS predictions, discretization of both the spatial and spectral integrations must be performed carefully in order to ensure accurate results. In particular, it is well known that evaluation of KA NRCS predictions becomes difficult numerically as the surface rms height increases, due to the rapid decrease in the integrand near the origin. A sufficient number of spatial integration points must be utilized to model such cases accurately. When using an FFT algorithm, the spectral discretization is determined by the spatial discretization according to standard FFT rules. However, due to the inclusion of the second order SPM kernel functions in the RLCA3 kernel, it is possible for the RLCA3 kernel to exhibit rapid variations with its argument in some cases. These variations become more pronounced as the dielectric constant or conductivity of the lower region becomes larger; reference [11] provides further discussion of this point. In such cases, sufficient spectral discretization must be retained in order to ensure that rapid kernel function variations are resolved. Both spectral and spatial discretization issues can typically be examined simply by seeking convergence of predictions as the discretization rate is increased.

The results to be presented in the next section were obtained through a direct discretization of the integrals in equations (33)-(35), along with an FFT algorithm for evaluation of equations (40)-(41). Integrations were performed over a spatial grid of 32 by 32 wavelengths, sampled into 512 by 512 points. Computation of all three NRCS terms in all four polarization combinations required approximately 23 seconds per angle on an 800 MHz Pentium processor.

VI. Example RLCA3 predictions

Results are first illustrated to compare RLCA3 predictions with those of the two field series term SSA and LCA3 [9] theories. Surfaces are modeled as Gaussian stochastic processes with an isotropic Gaussian correlation function, so that surface statistics are completely specified by the rms height (h_0) and correlation length (l) parameters; this type of rough surface will be referred to as a "Gaussian" surface in what follows. Results are also compared with those from a Monte Carlo simulation using the method of moments (MOM). The latter utilized 50 realizations, and results were computed using the canonical grid technique [12] in a four scalar function unknown method of moments for a penetrable surface [13] to improve computational efficiency. MOM surfaces sizes were $16\lambda \times 16\lambda$ sampled in 128×128 points, and the "tapered" incident field described in [12] with $g = 5$ was used to eliminate edge scattering effects. Note use of the tapered incident field causes inaccuracies for large bistatic scattering angles and for cross-polarized predictions, so method of moments results are only included for co-polarized predictions at scattering angles within 70 degrees. Computational times for this numerical approach were dramatically larger (on the order of tens of CPU hours) compared to those required for the RLCA3. To make the results shown comparable to those in the literature, kernel functions are transformed from the original polarization basis (equation (7)) to the local polarization basis (equation (51) in the appendix) in the computations.

Figure 1 illustrates in-plane bistatic NRCS predictions for $Kh_0 = 1$, $Kl = 6$, and surface relative permittivity $\epsilon = 4 + i$. The incident field impinges upon the surface at $\theta_i = 30^\circ$ from normal incidence, and the polar scattering angle used in the figure is defined so that $\theta_s = 30^\circ$ is specular scattering while $\theta_s = -30^\circ$ is backscattering. Results in all four NRCS polarizations are plotted: again the second index of the $\alpha\beta$ notation (hv for example) indicates the incident polarization. Co-polarized (hh and vv) results show little difference between the SSA2, two-term LCA3 theory (labeled "LCA2") of [9], and the RLCA3 theories, and all are in good agreement with the MOM simulation. The RLCA3 corrects a slight over-prediction of HH cross sections by the LCA2 at large bistatic scattering angles. A larger difference among theories is observed in cross polarized predictions; here the RLCA3 shows significantly larger predicted cross sections than the LCA2 theory, in agreement with the SSA. Note all cross-polarized predictions are obtained from the second field series term, as the KA1 prediction for cross-polarized NRCS vanishes in the plane of incidence. These results clearly demonstrate the importance of the $\mathbf{B}_2$ kernel in cross polarized predictions; although numerical results for cross polarization are not shown, SSA predictions of cross polarized scattering have been verified in other studies.

Figure 2 is analogous to Figure 1, but for the case $Kh_0 = 0.5$ and $Kl = 3$ (i.e. the frequency has been decreased by a factor of two.) Results in terms of relationships among theories are generally similar. Note the small MOM predictions obtained near specular angles are due to difficulties in removing the coherent scattered field in the numerical simulation, and should not be taken as accurate.

The preceding cases show close agreement of the SSA and RLCA3 predictions. Figure 3 illustrates a case where the two theories show appreciable differences. Here the surface parameters are $Kh_0 = \pi$, $Kl = 4\pi$, $\epsilon = 25 + i3$, and the incidence angle is 20 degrees. This case was previously considered in [14], and the numerical results plotted are obtained from the authors of [14] rather than from the MOM simulations discussed previously. General conclusions are similar regarding the relationships among theories, although for this case, the cross polarized cross sections of SSA and RLCA3 show some unusual angular dependencies that cannot be verified here due to continued corruption of the numerical cross-polarized predictions. The vv plot however shows a significant deviation of SSA predictions from the numerical model at both large negative and positive scattering angles. These deviations have been attributed in part to the influence of the near-singular

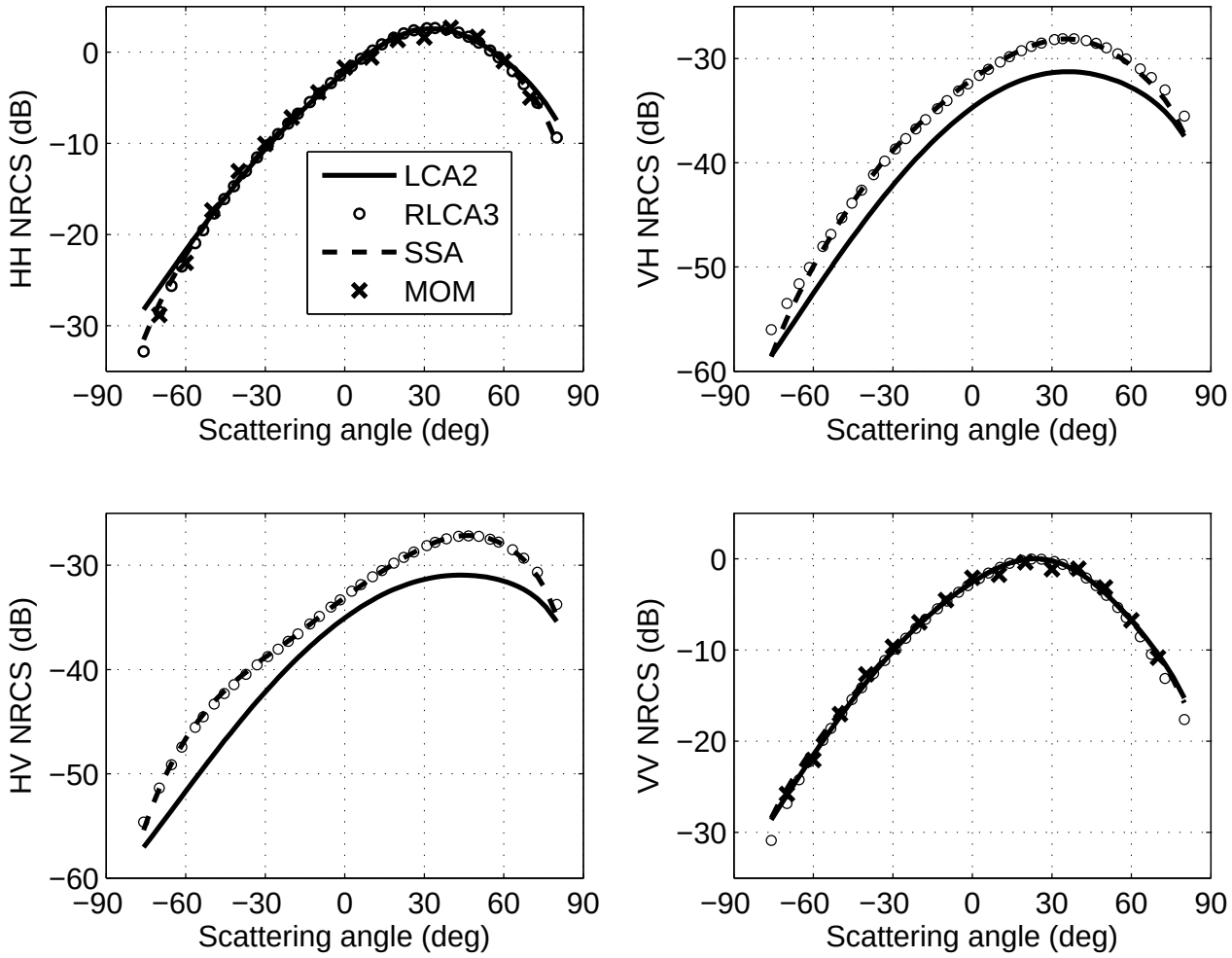

Fig. 1. Normalized radar cross sections for a Gaussian rough surface, $Kh_0 = 1$, $Kl = 6$, $\epsilon = 4 + i$, $\theta_i = 30^\circ$

portion of the vv B2 kernel function. In addition, the failure of the SSA model to approach KA identically has impact upon these results. The RLCA3 prediction reduces these problems so that better agreement with the numerical model is achieved.

VII. Extensions of the RLCA3 and SSA theories

An extension of the RLCA3 model is possible that allows the SPM1 limit to be reached to arbitrary order in surface tilt, rather than first order. This extension involves adding the term

$$-\frac{1}{2}\mathbf{T}_2(\boldsymbol{K}, \boldsymbol{K}_0; \hat{x}\xi_x + \hat{y}\xi_y, -Q_z \nabla h) \tag{43}$$

to the $\mathbf{T}_1^{'}$ kernel function in equation (13). Here ∇h refers to the spatial derivative of the surface profile function. This correction can be derived in a manner similar to the process used for transforming the original LCA theory to the "weighted curvature approximation" in [8]. It can be shown that this addition still results in the total field solution matching the KA, untilted SPM1, and untilted SPM2, while improving the tilt properties of the SPM1 to arbitrary order in surface tilt. The disadvantage of this modification is the fact that the RLCA3 kernel function now becomes dependent on the local surface slope. In this case, the spectral and spatial integrations in equation (13) can no longer be decoupled, so that a complete four dimensional integration is required to evaluate model predictions. The dramatically increased computational complexity of such a model makes its use less practical than the RLCA3 theory without this correction.

A second result derived in the development of the RLCA3 theory involves a method for improving the standard SSA theory to ensure that the KA limit is reached. In the standard SSA theory, $\boldsymbol{\mathcal{K}}(\boldsymbol{K}, \boldsymbol{K}_0)$ in equation (12) is replaced with $\boldsymbol{\mathcal{B}}(\boldsymbol{K}, \boldsymbol{K}_0|\hat{z})$, and the $\mathbf{T}_1^{'}(\boldsymbol{K}, \boldsymbol{K}_0; \boldsymbol{\xi}, \boldsymbol{Q_H} - \boldsymbol{\xi})$ function in equation (13) is replaced with

$$\begin{aligned}\mathbf{M}(\boldsymbol{K}, \boldsymbol{K}_0; \boldsymbol{\xi}) \;=\; & \frac{1}{2}\left[\mathbf{B}_2\left(\boldsymbol{K}, \boldsymbol{K}_0; \boldsymbol{K} - \boldsymbol{\xi}|\hat{z}\right)\right. \\ & +\mathbf{B}_2\left(\boldsymbol{K}, \boldsymbol{K}_0; \boldsymbol{K}_0 + \boldsymbol{\xi}|\hat{z}\right) - \\ & \left.\mathbf{B}\left(\boldsymbol{K}, \boldsymbol{K}_0|\hat{z}\right)\right]\end{aligned} \tag{44}$$

where $\boldsymbol{\xi} = \hat{x}\xi_x + \hat{y}\xi_y$. The SSA matches the untilted SPM1 and SPM2 limits, as well as obtaining first order in slope tilt invariance for SPM1, but fails to match KA. Agreement with

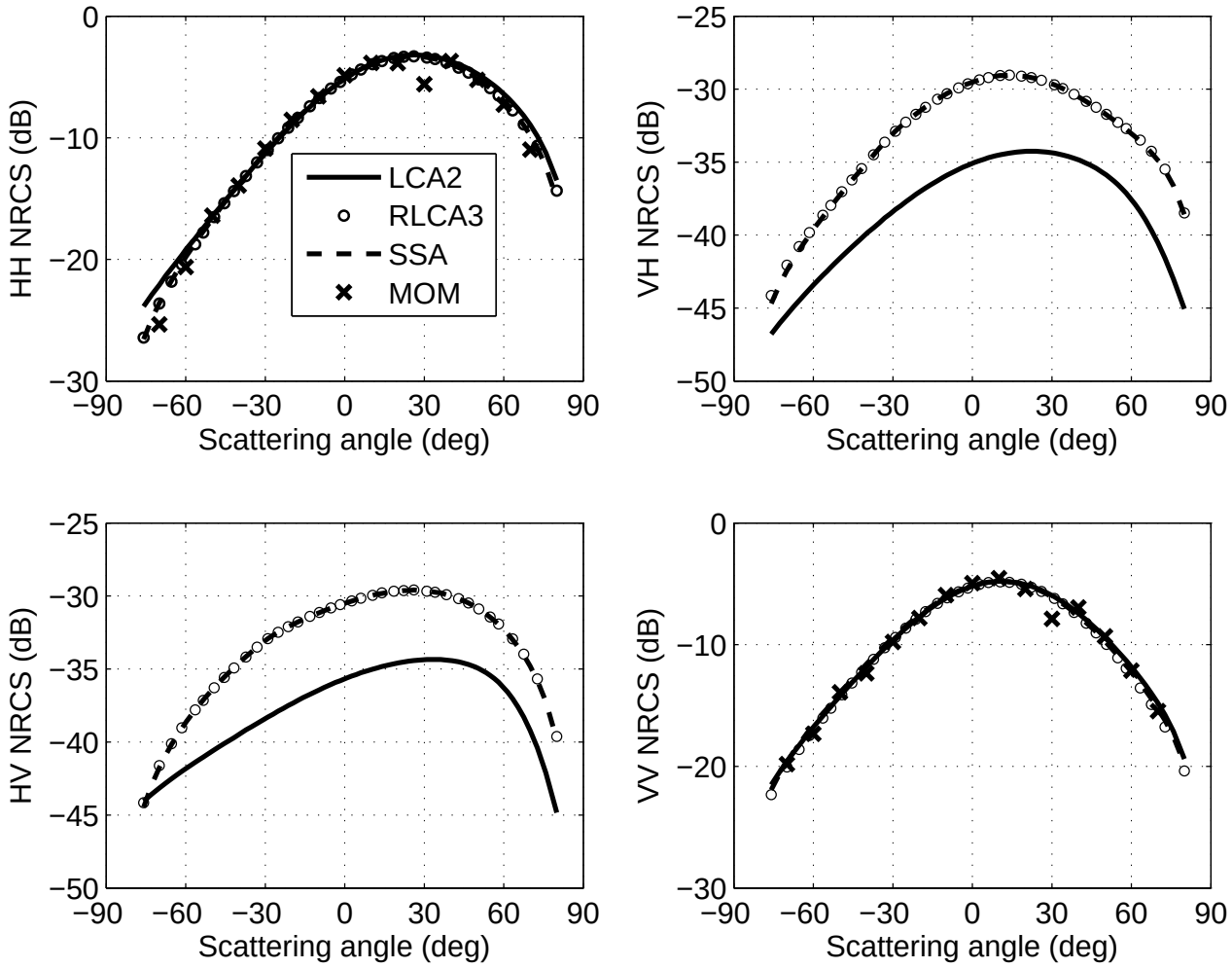

Fig. 2. Normalized radar cross sections for a Gaussian rough surface, $Kh_0 = 0.5$, $Kl = 3$, $\epsilon = 4 + i$, $\theta_i = 30^\circ$

the KA can be achieved by adding an additional kernel term

$$\begin{aligned}\Delta\mathbf{M}(\boldsymbol{K},\boldsymbol{K}_0;\boldsymbol{\xi}) &= \frac{1}{2}\left[\mathbf{T}_1(\boldsymbol{K},\boldsymbol{K}_0;\boldsymbol{Q}_H)\right. \\ &\quad \left(1+2\frac{\boldsymbol{W}_H}{W_z}\cdot\frac{\boldsymbol{\xi}}{Q_z}\right) \\ &+ \mathbf{T}_1(\boldsymbol{K},\boldsymbol{K}_0;\boldsymbol{\xi}) \\ &- \left.\mathbf{T}_1(\boldsymbol{K},\boldsymbol{K}_0;\boldsymbol{Q}_H-\boldsymbol{\xi})\right] \end{aligned} \quad (45)$$

to the standard SSA kernel function. In the above equation, the vector $\boldsymbol{W} = \boldsymbol{K} + \boldsymbol{K}_0$, and $\boldsymbol{W_H}$ and W_z refer to the horizontal and vertical parts of $\boldsymbol{W}$ respectively. This correction makes no contribution to the SPM1 or SPM2 limits, but corrects the Taylor series expansion of $\mathbf{M}$ in $\boldsymbol{\xi}$ so that the KA limit is achieved. Such a corrected SSA theory should have properties very similar to the RLCA3, although the full tilt invariance properties of the corrected SSA model have yet to be investigated.

One motivation for choice of the RLCA3 model over the corrected SSA is the use of the KA as the dominant series term. Due to the formal tilt invariance of the KA, such a choice may provide enhanced tilt invariance properties overall to RLCA3 predictions, at least as the high frequency limit is approached. In addition, the structure of the LCA theory results in the first correction to KA involving terms that are of the order of the surface second derivative. The RLCA3 model can be interpreted as further adding an additional expansion in the surface slope squared. For one dimensional surfaces, this combination can be regarded as the RLCA3 theory performing an expansion based on the surface intrinsic, rather than local, curvature. Because the intrinsic curvature is coordinate system independent, such an expansion again should have a better chance of achieving significant tilt invariance properties.

VIII. Conclusions

This paper has presented the RLCA3 model for rough surface scattering, including explicit expressions both for scattered fields from a deterministic surface and for ensemble averaged normalized radar cross sections for a Gaussian random process surface. The model overall achieves compliance with the KA and with the SPM up to second order, with first order in slope tilt invariance of the SPM1. Sample results demonstrated that the RLCA3 produces predictions similar to the two-term SSA theory in many cases, although an example was shown in which the SSA showed apparent errors that were corrected by the RLCA3. Overall, the basic properties of the

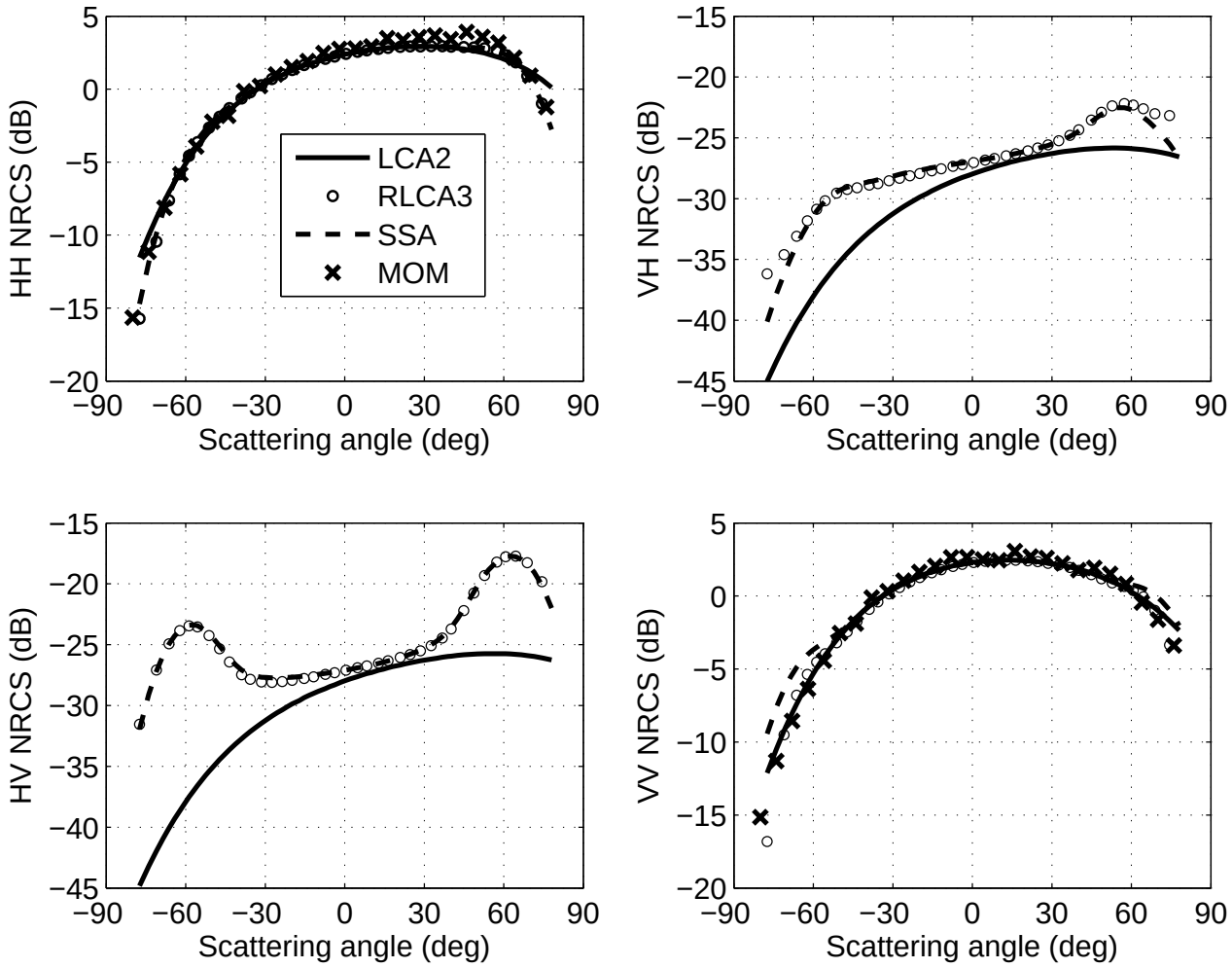

Fig. 3. Normalized radar cross sections for a Gaussian rough surface, $Kh_0 = \pi$, $Kl = 4\pi$, $\epsilon = 25 + i3$, $\theta_i = 20^\circ$

RLCA3 make the model attractive for use in further studies of rough surface scattering.

IX. Appendix

In the polarization basis of equations (3)-(6),

$$\begin{aligned}\boldsymbol{\mathcal{K}}(\boldsymbol{K},\boldsymbol{K}_0) &= \frac{-Q^2}{2}\Big(\hat{\boldsymbol{H}}_{\boldsymbol{s}} R_{HH}(Q/2)\hat{\boldsymbol{H}}_{\boldsymbol{i}} \\ &\quad +\hat{\boldsymbol{V}}_{\boldsymbol{s}} R_{VV}(Q/2)\hat{\boldsymbol{V}}_{\boldsymbol{i}}\Big) \end{aligned} \quad (46)$$

where

$$Q = |\boldsymbol{Q}| \quad (47)$$

$$R_{HH}(\beta) = \frac{\beta - \sqrt{(\epsilon-1)K^2+\beta^2}}{\beta + \sqrt{(\epsilon-1)K^2+\beta^2}} \quad (48)$$

$$R_{VV}(\beta) = \frac{\epsilon\beta - \sqrt{(\epsilon-1)K^2+\beta^2}}{\epsilon\beta + \sqrt{(\epsilon-1)K^2+\beta^2}} \quad (49)$$

Specification of the RLCA3 kernel function requires specification of the $\mathbf{B}(\boldsymbol{K},\boldsymbol{K}_0|\hat{\boldsymbol{n}})$ and $\mathbf{B}_2(\boldsymbol{K},\boldsymbol{K}_0;\boldsymbol{\xi}|\hat{\boldsymbol{n}})$ SPM kernel functions. Most references (for example [15]) utilize a polarization basis that depends on $\hat{\boldsymbol{n}}$ for reporting these kernels. This polarization basis is defined as:

$$\begin{aligned}\hat{\boldsymbol{h}}_i &= \hat{\boldsymbol{K_0}} \times \hat{\boldsymbol{n}} / \left|\hat{\boldsymbol{K_0}} \times \hat{\boldsymbol{n}}\right| \\ \hat{\boldsymbol{h}}_s &= \hat{\boldsymbol{K}} \times \hat{\boldsymbol{n}} / \left|\hat{\boldsymbol{K}} \times \hat{\boldsymbol{n}}\right| \\ \hat{\boldsymbol{v}}_i &= \hat{\boldsymbol{h}}_i \times \hat{\boldsymbol{K_0}} \\ \hat{\boldsymbol{v}}_s &= \hat{\boldsymbol{h}}_s \times \hat{\boldsymbol{K}} \end{aligned} \quad (50)$$

so that

$$\begin{aligned}\mathbf{S}(\boldsymbol{K},\boldsymbol{K}_0|\hat{\boldsymbol{n}}) &= \hat{\boldsymbol{h}}_s S_{hh}\hat{\boldsymbol{h}}_i + \hat{\boldsymbol{v}}_s S_{vh}\hat{\boldsymbol{h}}_i \\ &+ \hat{\boldsymbol{h}}_s S_{hv}\hat{\boldsymbol{v}}_i + \hat{\boldsymbol{v}}_s S_{vv}\hat{\boldsymbol{v}}_i \end{aligned} \quad (51)$$

However the above dyad can be transformed easily to the

$(\hat{\boldsymbol{H}}, \hat{\boldsymbol{V}})$ basis by substituting

$$\hat{\boldsymbol{h}}_i = \left(\frac{\hat{\boldsymbol{n}} \cdot \hat{\boldsymbol{V}}_{\boldsymbol{i}}}{\left|\hat{\boldsymbol{n}} \times \hat{\boldsymbol{K}}_{\boldsymbol{0}}\right|}\right) \hat{\boldsymbol{H}}_{\boldsymbol{i}} - \left(\frac{\hat{\boldsymbol{n}} \cdot \hat{\boldsymbol{H}}_{\boldsymbol{i}}}{\left|\hat{\boldsymbol{n}} \times \hat{\boldsymbol{K}}_{\boldsymbol{0}}\right|}\right) \hat{\boldsymbol{V}}_{\boldsymbol{i}} \quad (52)$$

$$\hat{\boldsymbol{h}}_s = \left(\frac{\hat{\boldsymbol{n}} \cdot \hat{\boldsymbol{V}}_{\boldsymbol{s}}}{\left|\hat{\boldsymbol{n}} \times \hat{\boldsymbol{K}}\right|}\right) \hat{\boldsymbol{H}}_{\boldsymbol{s}} - \left(\frac{\hat{\boldsymbol{n}} \cdot \hat{\boldsymbol{H}}_{\boldsymbol{s}}}{\left|\hat{\boldsymbol{n}} \times \hat{\boldsymbol{K}}\right|}\right) \hat{\boldsymbol{V}}_{\boldsymbol{s}} \quad (53)$$

$$\hat{\boldsymbol{v}}_i = \left(\frac{\hat{\boldsymbol{n}} \cdot \hat{\boldsymbol{H}}_{\boldsymbol{i}}}{\left|\hat{\boldsymbol{n}} \times \hat{\boldsymbol{K}}_{\boldsymbol{0}}\right|}\right) \hat{\boldsymbol{H}}_{\boldsymbol{i}} + \left(\frac{\hat{\boldsymbol{n}} \cdot \hat{\boldsymbol{V}}_{\boldsymbol{i}}}{\left|\hat{\boldsymbol{n}} \times \hat{\boldsymbol{K}}_{\boldsymbol{0}}\right|}\right) \hat{\boldsymbol{V}}_{\boldsymbol{i}} \quad (54)$$

$$\hat{\boldsymbol{v}}_s = \left(\frac{\hat{\boldsymbol{n}} \cdot \hat{\boldsymbol{H}}_{\boldsymbol{s}}}{\left|\hat{\boldsymbol{n}} \times \hat{\boldsymbol{K}}\right|}\right) \hat{\boldsymbol{H}}_{\boldsymbol{s}} + \left(\frac{\hat{\boldsymbol{n}} \cdot \hat{\boldsymbol{V}}_{\boldsymbol{s}}}{\left|\hat{\boldsymbol{n}} \times \hat{\boldsymbol{K}}\right|}\right) \hat{\boldsymbol{V}}_{\boldsymbol{s}} \quad (55)$$

and recombining pairs of vectors to obtain the form of equation (7). This process is to be utilized when computing the $\mathbf{B}$ and $\mathbf{B}_2$ kernels used, as all dyad's are to be written in the global polarization basis of equations (3)-(6).

In the local polarization basis, the first order SPM kernel functions are specified as:

$$B_{hh}(\boldsymbol{K}, \boldsymbol{K}_0|\hat{\boldsymbol{n}}) = \frac{2q_k q_0 (\epsilon - 1) K^2 \hat{\boldsymbol{k}} \cdot \hat{\boldsymbol{k}}_0}{\left(q_k + q_k^{'}\right)\left(q_0 + q_0^{'}\right)} \quad (56)$$

$$B_{vh}(\boldsymbol{K}, \boldsymbol{K}_0|\hat{\boldsymbol{n}}) = \frac{2q_k q_0 (\epsilon - 1) K^2}{\left(\epsilon q_k + q_k^{'}\right)\left(q_0 + q_0^{'}\right)} \frac{q_k^{'}}{K} \left(\hat{\boldsymbol{n}} \cdot \left(\hat{\boldsymbol{k}}_0 \times \hat{\boldsymbol{k}}\right)\right) \quad (57)$$

$$B_{hv}(\boldsymbol{K}, \boldsymbol{K}_0|\hat{\boldsymbol{n}}) = \frac{2q_k q_0 (\epsilon - 1) K^2}{\left(q_k + q_k^{'}\right)\left(\epsilon q_0 + q_0^{'}\right)} \frac{q_0^{'}}{K} \left(\hat{\boldsymbol{n}} \cdot \left(\hat{\boldsymbol{k}}_0 \times \hat{\boldsymbol{k}}\right)\right) \quad (58)$$

$$B_{vv}(\boldsymbol{K}, \boldsymbol{K}_0|\hat{\boldsymbol{n}}) = \frac{2q_k q_0 (\epsilon - 1) K^2}{\left(\epsilon q_k + q_k^{'}\right)\left(\epsilon q_0 + q_0^{'}\right)} \frac{\left(\epsilon |\boldsymbol{k}| |\boldsymbol{k}_0| - q_k^{'} q_0^{'} \hat{\boldsymbol{k}} \cdot \hat{\boldsymbol{k}}_0\right)}{K^2} \quad (59)$$

where

$$q_k = \hat{\boldsymbol{n}} \cdot \boldsymbol{K} \quad (60)$$

$$q_0 = -\hat{\boldsymbol{n}} \cdot \boldsymbol{K}_0 \quad (61)$$

$$\boldsymbol{k} = \mathbf{P}_{\parallel}(\hat{\boldsymbol{n}}) \cdot \boldsymbol{K} \quad (62)$$

$$\boldsymbol{k}_0 = \mathbf{P}_{\parallel}(\hat{\boldsymbol{n}}) \cdot \boldsymbol{K}_0 \quad (63)$$

$$q_k^{'} = \sqrt{\epsilon K^2 - \boldsymbol{k} \cdot \boldsymbol{k}} \quad (64)$$

$$q_0^{'} = \sqrt{\epsilon K^2 - \boldsymbol{k}_0 \cdot \boldsymbol{k}_0} \quad (65)$$

The second order SPM kernel functions are specified as

$$B_{2,hh}(\boldsymbol{K}, \boldsymbol{K}_0; \boldsymbol{\xi}|\hat{\boldsymbol{n}}) = \frac{2q_k q_0 (\epsilon - 1) K^2}{Q_n \left(q_k + q_k^{'}\right)\left(q_0 + q_0^{'}\right)} \Bigg\{ C_1 C_2 \left(R_1 + q_k^{'}\right) + S_1 S_2 \left(q_k^{'} + R_2\right) + \frac{C_3}{2}\left(q_0^{'} - q_k^{'}\right) \Bigg\} \quad (66)$$

$$B_{2,vh}(\boldsymbol{K}, \boldsymbol{K}_0; \boldsymbol{\xi}|\hat{\boldsymbol{n}}) = \frac{2q_k q_0 (\epsilon - 1) K^2}{Q_n \left(\epsilon q_k + q_k^{'}\right)\left(q_0 + q_0^{'}\right)} \Bigg\{ S_1 C_2 \left(\epsilon K + \frac{q_k^{'}}{K} R_1\right) - C_1 S_2 \left(\epsilon K + \frac{q_k^{'}}{K} R_2\right) + S_2 \frac{\epsilon |\boldsymbol{k}|}{K} R_3 + \frac{S_3}{2}\left(\epsilon K - \frac{q_k^{'}}{K} q_0^{'}\right) \Bigg\} \quad (67)$$

$$B_{2,hv}(\boldsymbol{K}, \boldsymbol{K}_0; \boldsymbol{\xi}|\hat{\boldsymbol{n}}) = \frac{2q_k q_0 (\epsilon - 1) K^2}{Q_n \left(q_k + q_k^{'}\right)\left(\epsilon q_0 + q_0^{'}\right)} \Bigg\{ -C_1 S_2 \left(\frac{q_0^{'}}{K}\right)\left(R_1 + q_k^{'}\right) + S_1 C_2 \left(\frac{q_0^{'}}{K}\right)\left(q_k^{'} + R_2\right) - S_1 \left(\frac{\epsilon |\boldsymbol{k}_0|}{K}\right) R_3 - \frac{S_3}{2}\left(\epsilon K - \frac{q_k^{'}}{K} q_0^{'}\right) \Bigg\} \quad (68)$$

(69)

$$B_{2,vv}(\boldsymbol{K}, \boldsymbol{K}_0; \boldsymbol{\xi}|\hat{\boldsymbol{n}}) = \frac{2q_k q_0 (\epsilon - 1) K^2}{Q_n \left(\epsilon q_k + q_k^{'}\right)\left(\epsilon q_0 + q_0^{'}\right)} \Bigg\{ -S_1 S_2 \left(\frac{q_0^{'}}{K}\right)\left(\epsilon K + \frac{q_k^{'}}{K} R_1\right) - C_1 C_2 \left(\frac{q_0^{'}}{K}\right)\left(\epsilon K + \frac{q_k^{'}}{K} R_2\right) + C_1 \left(\frac{\epsilon |\boldsymbol{k}_0| q_k^{'}}{K^2}\right) R_3 + \left(\frac{\epsilon |\boldsymbol{k}| R_3}{K^2}\right)\left(q_0^{'} C_2 + \frac{|\boldsymbol{\chi}| |\boldsymbol{k}_0|}{K^2} R_1\right) + \frac{C_3}{2}\left(\epsilon q_0^{'} - \epsilon q_k^{'}\right) \Bigg\} \quad (70)$$

where

$$\boldsymbol{\chi} = \mathbf{P}_{\parallel}(\hat{\boldsymbol{n}}) \cdot \boldsymbol{\xi} \quad (71)$$

$$q_\chi = \sqrt{K^2 - \boldsymbol{\chi} \cdot \boldsymbol{\chi}} \quad (72)$$

$$q_\chi^{'} = \sqrt{\epsilon K^2 - \boldsymbol{\chi} \cdot \boldsymbol{\chi}} \quad (73)$$

$$R_1 = q_\chi - q_\chi^{'} \quad (74)$$

$$R_2 = \frac{q_\chi q_\chi^{'} (1-\epsilon)}{\epsilon q_\chi + q_\chi^{'}} \quad (75)$$

$$R_3 = \frac{|\boldsymbol{\chi}| K^2}{|\boldsymbol{\chi}|^2 + q_\chi q_\chi^{'}} \quad (76)$$

$$C_1 = \hat{\boldsymbol{\chi}} \cdot \hat{\boldsymbol{k}} \quad (77)$$

$$C_2 = \hat{\boldsymbol{\chi}} \cdot \hat{\boldsymbol{k}}_0 \quad (78)$$

$$C_3 = \hat{\boldsymbol{k}} \cdot \hat{\boldsymbol{k}}_0 \quad (79)$$

$$S_1 = \hat{\boldsymbol{n}} \cdot \left(\hat{\boldsymbol{\chi}} \times \hat{\boldsymbol{k}} \right) \quad (80)$$

$$S_2 = \hat{\boldsymbol{n}} \cdot \left(\hat{\boldsymbol{\chi}} \times \hat{\boldsymbol{k}}_0 \right) \quad (81)$$

$$S_3 = \hat{\boldsymbol{n}} \cdot \left(\hat{\boldsymbol{k}} \times \hat{\boldsymbol{k}}_0 \right) \quad (82)$$

and $\boldsymbol{\xi}$ is an arbitrary three dimensional vector. The definitions of equations (60)-(65) are also used above.

One issue involved in computing the $\mathbf{T}_1$ kernel (which includes the $\mathbf{B}$ kernel evaluated in a tilted frame of reference) occurs when the tilting used is such that the incidence or scattering directions become shadowed. These conditions are defined as q_0 or q_k becoming negative, respectively. When these conditions occur, the $\mathbf{B}$ contributions to $\mathbf{T}_1$ are set to zero. This specification results in no discontinuities being introduced in $\mathbf{T}_1$ as the shadowed region is approached.

REFERENCES

[1] T. M. Elfouhaily and C. A. Guérin, "A critical survey of approximate scattering wave theories from random rough surfaces," *Waves in Random Media*, vol. 14, pp. R1–R40, 2004.

[2] A. G. Voronovich, "Small-Slope Approximation in wave scattering from rough surfaces," *Sov. Phys. JETP*, vol. 62, no. 1, pp. 65–70, 1985.

[3] A. G. Voronovich, "Small-Slope Approximation for electromagnetic wave scattering at a rough interface of two dielectric half-spaces," *Waves in Random Media*, vol. 4, no. 3, pp. 337–367, 1994.

[4] A. G. Voronovich,, *Wave scattering from rough surfaces*, ser. Springer Series on Wave Phenomena. Springer, 1994.

[5] M. S. Gilbert and J. T. Johnson, "A study of the higher-order small-slope approximation for scattering from a Gaussian surface," *Waves in Random Media*, vol. 13, pp. 137–143, 2003.

[6] A. G. Voronovich, "The effect of the Modulation of Bragg Scattering in Small-Slope Approximation," *Waves in Random Media*, vol. 12, pp. 341–349, 2002.

[7] C.-A. Guérin and M. Saillard, "On the high-frequency limit of the second-order small-slope approximation," *Waves in Random Media*, vol. 13, pp. 75–88, 2003.

[8] T. Elfouhaily, S. Guignard, R. Awadallah, and D. R. Thompson, "Local and non-local curvature approximation: a new asymptotic theory for wave scattering," *Waves in Random Media*, vol. 13, no. 4, pp. 321–338, 2003.

[9] T. M. Elfouhaily and J. T. Johnson, "Extension of the local curvature approximation to third order and full tilt invariance," accepted by *Waves in Random and Complex Media*, 2006.

[10] T. Yang and S. L. Broschat, "A comparison of scattering model results fro two-dimensional randomly rough surfaces," *IEEE Trans. Ant. Prop.*, vol. 40, pp. 1505–1512, 1992.

[11] A. Darawankul and J. T. Johnson, "An improved method for evaluating higher-order series terms in the small slope approximation for rough surface scattering," *IEEE Antennas and Propagation/URSI Symposium*, conference proceedings, 2005.

[12] K. Pak, L. Tsang, and J. T. Johnson, "Numerical simulations and backscattering enhancement of electromagnetic waves from two-dimensional dielectric random rough surfaces with the sparse-matrix canonical grid method," *J. Opt. Soc. Am. A*, vol. 14, pp. 1515–1529, 1997.

[13] J. T. Johnson, R. T. Shin, J. A. Kong, L. Tsang, and K. Pak, "A numerical study of ocean polarimetric thermal emission," *IEEE Trans. Geosc. Rem. Sens.*, vol. 37, pp. 8–20, 1999.

[14] C. A. Guérin, G. Soriano, and T. Elfouhaily, "Weighted curvature approximation: numerical tests for 2D dielectric surfaces," *Waves in Random Media*, vol. 14, pp. 349–363, 2004.

[15] J. T. Johnson, "Third order small perturbation method for scattering from dielectric rough surfaces," *J. Opt. Soc. Am. A*, vol. 16, pp. 2720–2726, 1999.